Proceedings of: TURBO EXPO 2002
ASME Turbo Expo: Land, Sea & Air 2002
June 3-6, 2002, Amsterdam, The Netherlands

Revised Version of GT-2002-30415

FLUID DYNAMICS OF A PRE-SWIRL ROTOR-STATOR SYSTEM

Youyou Yan
Aero, Civil and Mechanical Engineering
City University, London
Northampton Square
London EC1V 0HB, UK

Mahmood Farzaneh Gord
Department of Mechanical Engineering
University of Bath
Bath BA2 7AY, UK

Gary D Lock
Department of Mechanical Engineering
University of Bath
Bath BA2 7AY, UK

Michael Wilson
Department of Mechanical Engineering
University of Bath
Bath BA2 7AY, UK

J Michael Owen
Department of Mechanical Engineering
University of Bath
Bath BA2 7AY, UK

ABSTRACT

In a "direct-transfer" pre-swirl supply system, cooling air flows axially across the wheel-space from stationary pre-swirl nozzles to receiver holes located at a similar radius in the rotating turbine disc. This paper describes a combined computational and experimental study of the fluid dynamics of such a system.

Measurements of total and static pressures have been made using a purpose-built rotor-stator rig, with 24 pre-swirl nozzles on the stator and 60 receiver holes in the rotor. The number of pre-swirl nozzles could be reduced, and it was possible to calculate C_D, the discharge coefficient of the receiver holes. Information on the flowfield was also obtained from three-dimensional, incompressible steady turbulent flow computations.

The measurements showed that there was a significant loss of total pressure between the outlet from the pre-swirl nozzles and the rotating core of fluid in the wheel-space. This loss increased as the pre-swirl flow-rate and inlet swirl ratio increased, and as the number of nozzles decreased. C_D increased as the swirl ratio at the receiver hole radius approached unity; also C_D decreased as the number of nozzles decreased.

Computed pressures and tangential velocities were in mainly good agreement with the measurements. The computations help to explain the reasons for the significant losses in total pressure and for the relatively low values of C_D in this pre-swirl system.

Keywords: pre-swirl, rotor-stator systems, fluid dynamics, discharge coefficients

NOMENCLATURE

A	area
a	inner radius of cavity
b	outer radius of cavity
c	constant for calculation of β_p
C	constant (in equation 3)
C_D	discharge coefficient of receiver holes
c_p, c_v	specific heat at constant pressure and constant volume, respectively
C_w	nondimensional mass flow rate ($= \dot{m}\,\mu b$)
d	pre-swirl nozzle diameter
G	gap ratio (= s/b)
k	turbulence kinetic energy
$\dot{m}$	mass flow rate
N	number of pre-swirl nozzles
p	static pressure
p_0	total pressure in stationary frame
r, ϕ, z	radial, tangential and axial coordinates
Re_ϕ	rotational Reynolds number $\left(= \rho\Omega b^2/\mu\right)$
s	axial spacing between rotor and stator
T	temperature
U	total velocity in stationary frame
U_τ	friction velocity $(= \sqrt{\tau_w/\rho})$

V_r, V_ϕ, V_z	time-averaged radial, circumferential, axial components of velocity in stationary frame
$\dot{W}$	work done by fluid
x	nondimensional radius (= r/b)
y , y^+	distance normal to the wall , nondimensional distance (= $\rho y U_\tau/\mu$)
β	swirl ratio (= $V_\phi/\Omega r$)
β_p	pre-swirl ratio (= $V_{\phi,p}/\Omega r_p$)
ε	turbulent energy dissipation rate
γ	ratio of specific heats (= c_p/c_v)
λ_T	turbulent flow parameter (= $C_w/Re_\phi^{0.8}$)
θ	angle of pre-swirl nozzle to tangential direction
μ	dynamic viscosity
ρ	density
τ	shear stress
Ω	angular speed of disc

Subscripts

b	blade-cooling air, receiver hole radius
e	external air
eff	effective value
i	isentropic value
N	nozzles
o	total value in stationary frame of reference
p	pre-swirl air
R	receiver holes
s	sealing air
t	total value in rotating frame of reference
∞	value in core outside boundary layers
1,2	upstream, downstream stations in a stream tube

INTRODUCTION

The air used for internal cooling of turbine blades in engines is supplied through receiver holes near the periphery of the rotating turbine disc. The air is delivered across the wheelspace from "pre-swirl" nozzles, in the stator, angled to impart swirl to the air in the direction of rotation, thus reducing the relative temperature of the air entering the receiver holes. Fluid dynamics parameters of interest to the designer include the *effective* pre-swirl ratio, the loss of total pressure in the system and the discharge coefficients.

In some engines, as illustrated in Fig. 1a, the pre-swirl nozzles are located at a low radius on the stator, and the cooling air flows radially outward to the receiver holes through the rotating cavity between the disc and a rotating cover-plate attached to it. The flow in cover-plate systems has been studied computationally by Popp et al (1) and both experimentally and computationally by Karabay et al (2,3). Popp et al studied the geometric factors affecting the collection of the pre-swirl air at the base of the cover-plate, and made comparisons with system efficiencies measured by Meierhofer and Franklin (4). Karabay et al found that, at the high cooling air flow rates expected in engines, free-vortex flow occurs in the rotating cavity between the cover-plate and the disc; the adiabatic effectiveness of the system is then amenable to simplified theoretical analysis. The most important parameters affecting the flow structure were found to be the inlet pre-swirl ratio, $\beta_p = V_{\phi,p}/\Omega r_p$ (the ratio of the tangential component of velocity of the pre-swirl air to the speed of the rotating disc at the same radius) and the turbulent flow parameter, $\lambda_T = C_{W,p}Re_\phi^{-0.8}$, where $C_{W,p}$ is the nondimensional flow rate of the pre-swirl air and Re_ϕ is the rotational Reynolds number for the disc.

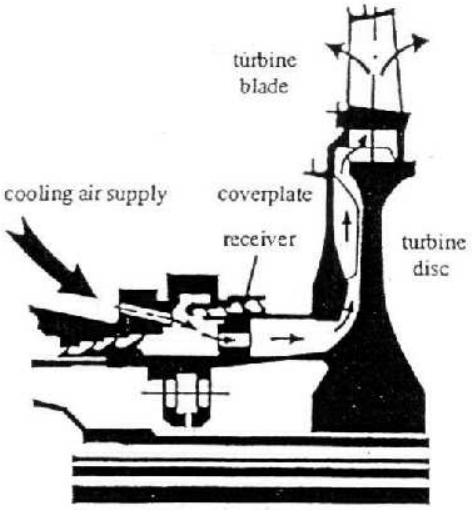

Fig. 1a A cover-plate pre-swirl system (reproduced from Popp et al, 1)

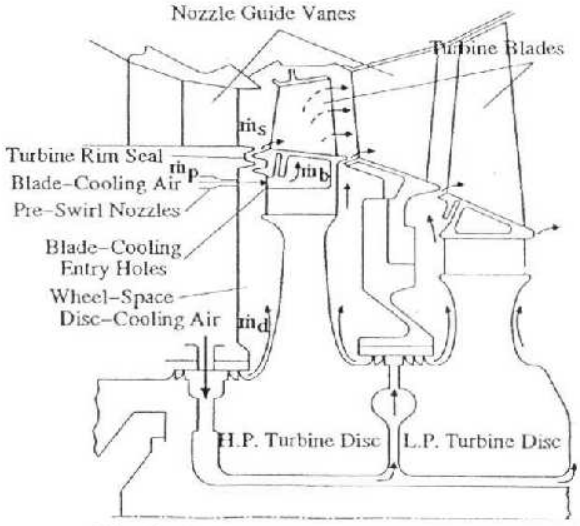

Fig. 1b A direct-transfer pre-swirl system (reproduced from Wilson et al, 5)

Karabay et al (2,3) found that the "effective" pre-swirl ratio, $\beta_{p,eff}$, for the radial outflow at the base of the cavity (at radius a close to that of the nozzles) was less than β_p. The difference is caused by mixing losses, which in cover-plate systems occur mainly as the inlet flow is turned radially as it enters the cavity. Karabay et al found that the ratio $\beta_{p,eff}$ / β_p reduces as β_p increases, and the free-vortex flow in the cover-plate cavity could then be represented by:

$$\frac{V_\phi}{\Omega r} = \beta_{p,eff}\left(\frac{x_P}{x}\right)^2 = \beta_p\left(\frac{\beta_{p,eff}}{\beta_p}\right)\left(\frac{x_p}{x}\right)^2 \qquad (1)$$

An alternative "direct-transfer" pre-swirl arrangement is used in other engines, as shown in Fig. 1b. In this system the stationary pre-swirl nozzles are located at a higher radius, compared with cover-plate systems, and the pre-swirl air is confined, by the seals, to a compact rotor-stator chamber in the outer part of the wheelspace. The flow and heat transfer in a model pre-swirl rotor-stator system was studied by Wilson et al (5), who found that the pre-swirl flow mixed fully with a superposed radial outflow of disc-cooling air before entering the receiver holes. Dittman et al (6) measured discharge coefficients for both the pre-swirl nozzles and the receiver holes in a direct transfer pre-swirl rig. Greater losses in total pressures are expected for direct transfer systems compared with the free-vortex flow found in cover-plate systems, due to strong mixing between the pre-swirl flow and the recirculating rotor-stator flow in the chamber. Earlier research into direct transfer systems, and rotor-stator systems in general, is described by Owen and Rogers (7).

This paper describes a combined experimental and computational study of the fluid dynamics of the idealised pre-swirl rotor-stator chamber shown schematically in Fig. 2. The results are used to describe the flow structure in the chamber and the effects of the parameters β_p and $\lambda_{T,p}$, and N, the number of pre-swirl nozzles. Discharge coefficients for the rotating receiver holes are also presented and discussed.

Designers are also interested in the total temperature of the cooling air that enters the turbine blade cooling passages, and this will be affected by heat transfer from the turbine disc to the air. Heat transfer in the system considered here will be discussed in a future publication.

EXPERIMENTAL APPARATUS

A rotor-stator rig, purpose-built for both flow and heat transfer studies, was used for the measurements. The geometry, which was based on information obtained for existing engine designs, is illustrated schematically in Fig. 2.

The disc radius was b = 216 mm, and the principal dimensions gave the inner-to-outer radius ratio (a/b) as 0.67 and the gap ratio (s/b) as 0.051. The rotating disc was made from transparent polycarbonate, for the subsequent application of optical heat transfer measurements using liquid crystal techniques. There were 24 circular pre-swirl nozzles, angled at $\theta = 20°$ to the tangential direction, in the stator, and 60 axial receiver holes in the rotor; the receiver holes were square-edged with a length-to-diameter ratio of 1.25. The radial location of the nozzles, for which $x_p = r_p / b = 0.74$, was less than the centreline radius of the holes at $x_b = r_b / b = 0.93$ (Fig. 2). The number of pre-swirl nozzles, N, could be reduced from N = 24 to N = 12 by blocking every other nozzle, and this allowed higher inlet swirl ratios to be tested for the pre-swirl flow rates available. The ratio of the area of the receiver holes to that of the nozzles (A_R/A_N) was 2.9 for N = 24 and 5.8 for N = 12. The inlet swirl ratio, β_p, was calculated from:

$$\beta_p = \frac{C}{N}\left(\frac{C_{W,p}}{Re_\phi}\right) = \frac{C}{N}\lambda_{T,p}\,Re_\phi^{-0.2} \qquad (2)$$

where

$$C = \frac{4b^3\cos\theta}{\pi d^2 r_p} \qquad (3)$$

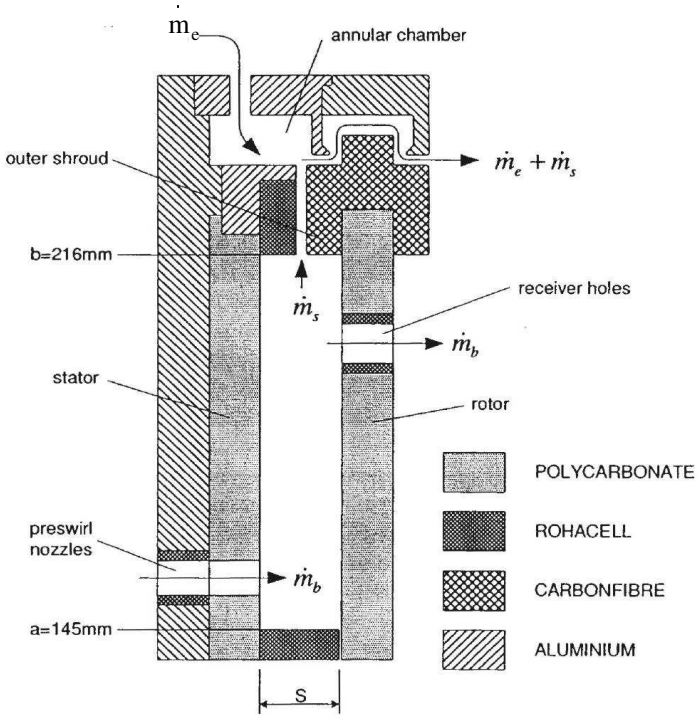

Fig. 2 Schematic diagram of the rotor-stator experimental rig (not to scale)

The outer shroud was in two sections, one attached to the stator and the other to the rotor; the inner shroud was stationary. A stationary annular chamber was fitted around the periphery of the system, and this chamber could be pressurised (by an external flow rate, $\dot{m}_e$) to control the seal flow rate, $\dot{m}_s$, through the peripheral seals. The value of $\dot{m}_s$ was determined from calibration tests of the seal assembly.

The rig could be rotated at speeds giving rotational Reynolds numbers Re_ϕ (based on the disc radius) up to around $1.2x10^6$. It was possible to control independently $\dot{m}_p$, m_b and $\dot{m}_s$, the pre-swirl, blade-cooling and sealing flow rates, respectively (see Fig. 2), and the mass flow rates were measured using British Standard orifice plates. Tests were carried out for sealing flow rates $C_{w,s}$ of zero and $C_{w,s} / C_{w,b} \approx 0.1$; only results for the former are included here.

A total-temperature probe and pitot-tube located in the outlet from the nozzles, together with a static-pressure tap between the nozzles, were used to measure the total and static temperature and the velocity of the inlet flow. (Equation (2), rather than the measured inlet velocity, was used to calculate β_p.) Static pressure taps were located at nine radial stations in the stator, and nine pitot-tubes were located at the same radii on the mid-axial plane (z/s = 0.5) in the wheel-space. This enabled the measurement of the radial distribution of p, the static pressure, p_o, the total pressure, and $V_{\phi,\infty}$, the tangential velocity of the air in the core outside the boundary layers. As the blade-cooling air discharged directly into the atmosphere, it was also possible to calculate C_D, the discharge coefficient of the receiver holes.

It should be noted that the above measurements were made at only one angular location. However, the pitot-tubes in the mid-axial plane were subject to a rotating core of fluid, which would tend to average-out any circumferential variation in total pressure.

The parameter range tested in the experiments was:

$0.77x10^6 < Re_\phi < 1.2x10^6$
$0.6x10^4 < C_{w,p} < 2.8x10^4$ (giving $0.12 < \lambda_{T,p} = C_{W,p}Re_\phi^{-0.8} < 0.4$)
$0.5 < \beta_p < 3$.

Owen and Rogers (7) have shown that the flow structure depends principally on β_p and λ_T and only weakly on Re_ϕ, and this result has been confirmed by Karabay et al (2,3) for cover-plate pre-swirl systems. Hence, although the values of Re_ϕ used here are lower than those (typically around 10^7) found in gas turbines, the flow structures are considered to be representative of those found in the cooling systems of engines.

It was not possible to vary β_p, $C_{w,p}$, Re_ϕ and N independently (see equation 2); for $\beta_p \le 1$, 24 nozzles were used, while tests with $\beta_p > 1.5$ were carried out using the 12-nozzle configuration. (Tests were carried out for $\beta_p \approx 1$ for both 12 and 24 nozzles, however in these cases there was also a factor of two difference in flow rate.)

COMPUTATIONAL MODEL

Computations were carried out using a 3D incompressible flow model, with one discrete pre-swirl nozzle on the stator and cyclic-symmetry boundary conditions applied at the tangential faces of the domain. Computations were carried out only for N = 24 (i.e. a 15° segment).

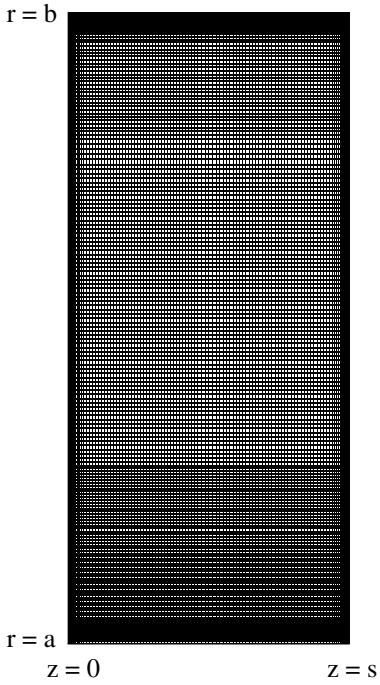

a) 140 x 211 axial x radial grid

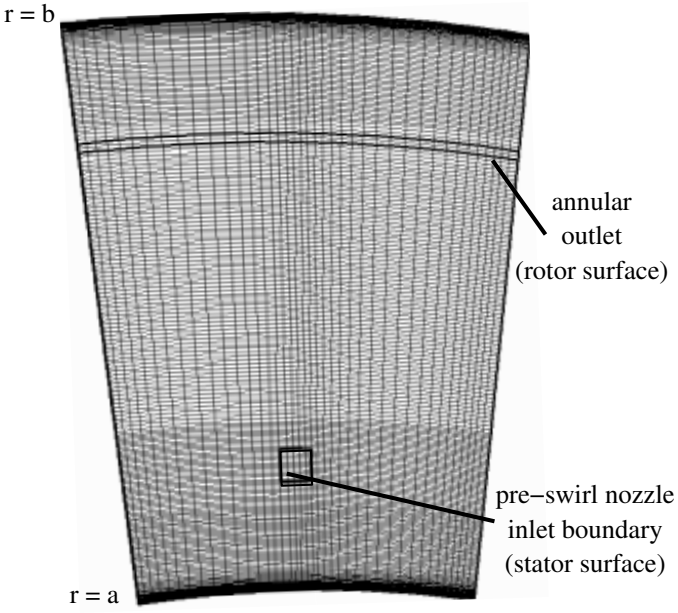

b) 211 x 40 radial x tangential grid

Fig. 3 140 x 211 x 40 computational grid

The structured cylindrical-polar mesh used is illustrated in Fig. 3. To permit steady-state computations, an annular outlet was used on the rotor that matched the centreline radius, r_b, and total flow area of the receiver holes. The Reynolds-averaged Navier-Stokes equations were solved in primitive-variable form using the finite-volume method, hybrid differencing and the SIMPLEC pressure-correction scheme. The low-Reynolds-number Launder-Sharma (8) k-ε turbulence model was used; this model has been used successfully in previous pre-swirl research where both flow and heat transfer is to be considered (see, for example, Pilbrow et al (9)). Grid distribution tests showed that a 140 × 211 × 40 (axial × radial × tangential) grid was required. Near wall grid points satisfied the condition y+ < 1, and a convergence condition that total absolute residuals be less than 10^{-4} when normalised by inlet mass flux and tangential velocity values was used.

Boundary conditions for the axial and tangential velocity components were prescribed for the angled flow at the inlet (which was square but having the same area as the circular nozzles in the rig), using the flow rates recorded in the experiments. The radial velocity component at inlet was zero. The angular velocity of the disc was also set to match the measured disc speed. At the annular outlet boundary on the rotating disc, a uniform normal velocity component based on measured flow rates was imposed to ensure continuity, and tangential velocities were computed from a zero normal derivative condition. (At the seal clearances, see Fig. 2, a linear variation in angular velocity between rotating and stationary components was used for the zero sealing flow cases.)

RESULTS

Computed flow structure

Figs. 4a and 4b show computed vector velocity fields, for $Re_\phi = 0.78x10^6$, $\lambda_{T,p} = 0.236$ and $\beta_p = 0.96$, for the flow in two planes: one through the middle of the pre-swirl inlet nozzle (Fig. 4a), and the other mid-way between nozzles (Fig. 4b). Fig. 4a shows that the axial flow of pre-swirl air impinges on the rotor and flows outward over the rotating disc; the disc boundary layer supplies the blade-cooling flow leaving the system at the annular outlet at x = 0.93. Fig. 4b shows very similar characteristics except at low radius in the region of the axial pre-swirl flow; in this plane, mid-way between the inlet nozzles, the flow close to the stator at around x = 0.74 (the nozzle radius) is affected by entrainment into the pre-swirl flow. There is mixing between the pre-swirl flow, the recirculating flow inward of the nozzles and the radially inward flow on the stator; this reduces the effective pre-swirl ratio. For z/s > 0.5 approx., the velocity fields in the two planes are very similar, indicating that the discrete-inlet flows have merged. Under the influence of the rotating disc, the flow becomes very nearly axisymmetric prior to turning radially to form the disc boundary layer.

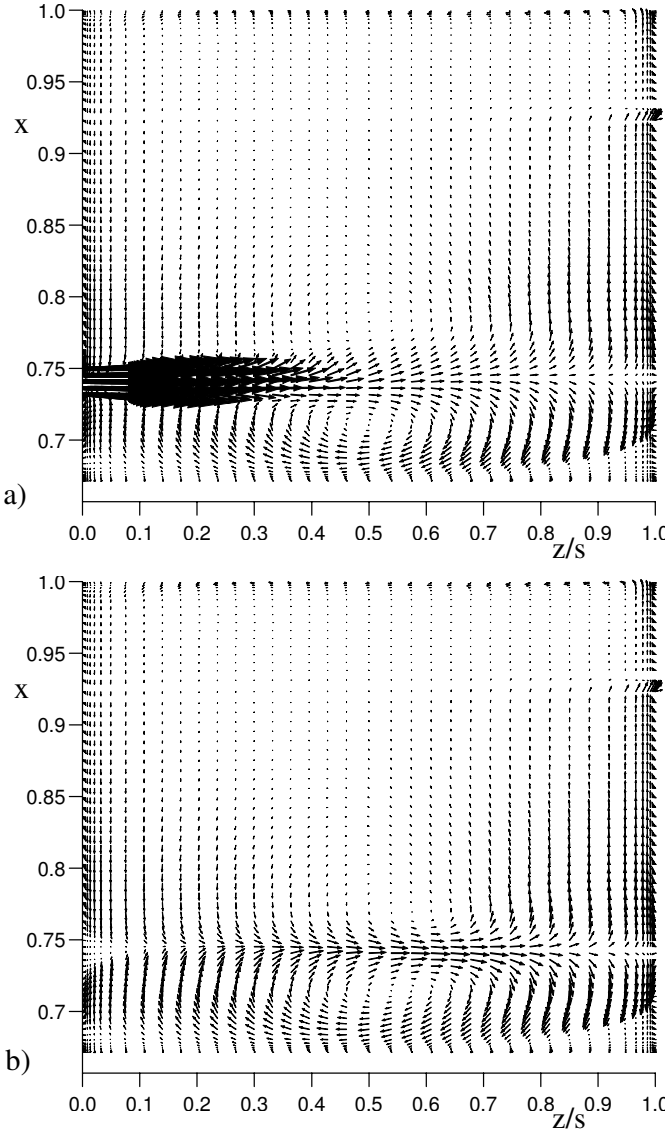

Fig. 4 Computed velocity vectors in two tangential planes for $Re_\phi = 0.78x10^6$, $\lambda_{T,p} = 0.236$ and $\beta_p = 0.96$
a) inlet nozzle mid-plane , b) mid-way between nozzles

Comparison between computations and measurements

Fig. 5a shows measured and computed stator-surface (z/s = 0) static pressures for three cases at $Re_\phi \approx 0.8x10^6$, with $\beta_p = 0.52$ (for which $\lambda_{T,p} = 0.127$) and $\beta_p = 0.96$ ($\lambda_{T,p} = 0.236$), both for N = 24, and $\beta_p = 1.86$ ($\lambda_{T,p} = 0.229$) for N = 12. (The computations shown for the latter case are for N = 24 at the same flow conditions; reliable solutions for N = 12 were not obtained due to increased gridding requirements.) Corresponding total pressures at the axial mid-plane (z/s = 0.5) are shown in Fig. 5b. The computed static pressures are the values obtained mid-way between inlet nozzles; the reference pressure for these incompressible flow

results was chosen arbitrarily as the measured static pressure at x = 0.9. There is reasonably good agreement between computed and measured values radially outward of the pre-swirl nozzles; inward of this location, the static pressure field is affected by the three-dimensional flow around the discrete nozzles. (Measurements were made on a radial line through the nozzle mid-plane.)

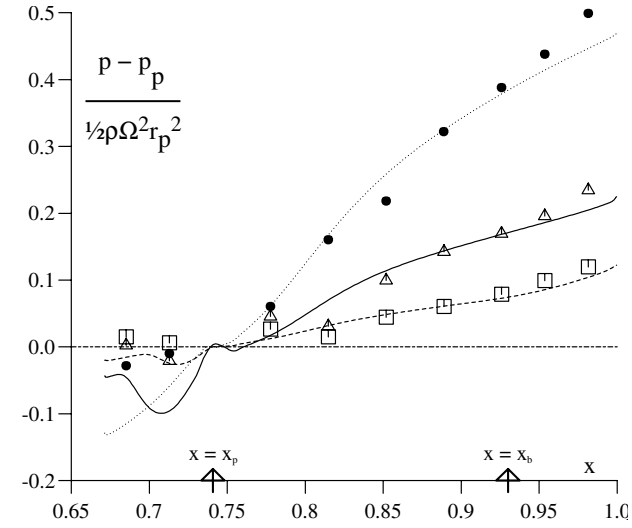

a) static pressure at stator surface

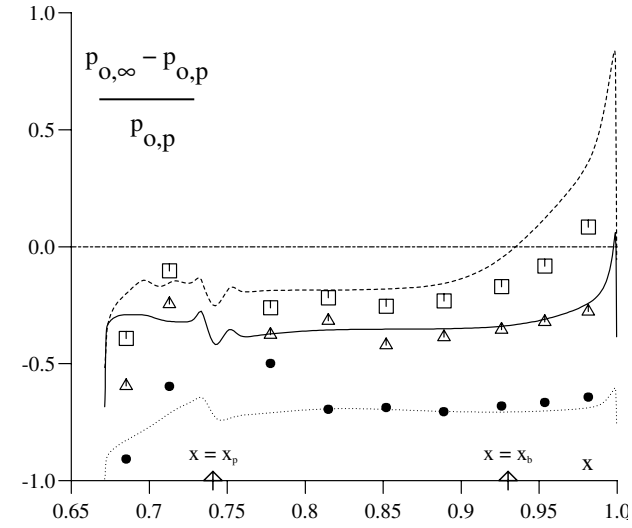

b) total pressure at axial mid−plane (z/s = 0.5)

Fig. 5 Measured and computed radial variation of pressure, $Re_\phi = 0.78x10^6$

measured — computed (N = 24)

- □ $\lambda_{T,p} = 0.127$, $\beta_p \approx 0.52$, N = 24 ------
- △ $\lambda_{T,p} = 0.236$, $\beta_p \approx 0.96$, N = 24 ——
- ● $\lambda_{T,p} = 0.229$, $\beta_p \approx 1.86$, N = 12 ·····

The mid-plane total pressure results, shown in Fig. 5b, are relative to the total pressure measured at the pre-swirl nozzle outlet. There are three noteworthy points: (i) owing to mixing losses, there is a significant drop in total pressure near the inlet (where $p_{0,\infty} < p_{0,p}$); (ii) except at the smaller or larger radii, $p_{0,\infty}$ is approximately constant, which is consistent with free-vortex flow; (iii) at the larger radii, the increase in $p_{0,\infty}$ is associated with work done on the air by the rotating disc and shroud. The tangentially-averaged computations generally show less variation with x than the data.

Fig. 6 shows measured distributions of β_∞ (= $V_{\phi,\infty}/\Omega r$) at z/s = 0.5 , obtained from the total and static pressure measurements, and computational results for the three inlet pre-swirl ratio cases discussed above (the values of β_p are indicated on the figure) at $Re_\phi \approx 0.8x10^6$. Fig. 6 also shows measured results for similar values of β_p obtained at a higher rotational Reynolds number, $Re_\phi \approx 1.18x10^6$, with the flow rate C_w adjusted so that $\lambda_{T,p}$ remained approximately constant for similar values of β_p. The measured results show that, as expected, there is no significant effect of Re_ϕ on the radial distribution of β_∞ for the lower values of β_p , and only a small effect on the magnitude of β_∞.

Not surprisingly, the results for β_∞ in Fig. 6 are consistent with those for $p_{0,\infty}$ in Fig. 5b. (i) The mixing losses near the inlet mean that $\beta_\infty < \beta_p$ at $x = x_p$ such that $\beta_{p,eff} < \beta_p$; (ii) except at the smaller or larger radii, β_∞ decreases as x increases: this is consistent with free-vortex flow in which $p_{0,\infty}$ is constant; (iii) at the larger radii, β_∞ increases as x increases as a consequence of work input from the rotating disc and shroud. (The tangential velocity at the boundary at z/s = 0.5, x = 1, in the computed results is less than that of the disc, as this point lies within the small clearance between the rotating and stationary sections of the shroud.)

The tangentially-averaged computed values of β_∞ for $\beta_p = 0.52$ in Fig. 6 show similar behaviour to the measurements. The computed level of β_∞ is in reasonable agreement with the data for x < 0.9, however the increase in β_∞ in the outer part of the system is overpredicted. The computational results are in good agreement with the data for $\beta_p = 0.96$ outward of the nozzle radius, $x_p = 0.74$. For $\beta_p = 1.86$, the computed distribution is qualitatively correct but the level of β_∞ is under-predicted. (As described above, this computation was carried out for N = 24, while the measurements correspond to N = 12.) The local minimum in β_∞ seen in the computed results at $x \approx 0.74$ occurs in the region just outward of the pre-swirl flow, where there is strong shear and entrainment into the jet flow (as illustrated in Fig. 4). For all the computed results, circumferential variations from the tangentially-averaged behaviour shown in Fig. 6 were very small except around the nozzle radius $x_p = 0.74$, where peak values of β_∞ for $\beta_p = 1.86$ were up to around 50% higher than the average values. No measurements were made of β_∞ at z/s = 0.5 at $x = x_p$.

The discharge coefficients for the receiver holes are expected to be affected by conditions near $x = x_b$ ($x_b = 0.93$), and Fig. 7

shows the measured variation of $\beta_{\infty,b}$ (i.e. at β_∞ at $x = x_b$), with β_p for N = 12 and N = 24; the measurements were made over a range of values of Re_ϕ and $\lambda_{T,p}$. The distributions are approximately linear:

$$N = 12\,(0.9 < \beta_p < 2.9):\ \beta_{\infty,b} \approx 0.1 + 0.28\,\beta_p \qquad (4a)$$

$$N = 24\,(0.5 < \beta_p < 1.5):\ \beta_{\infty,b} \approx 0.1 + 0.34\,\beta_p \qquad (4b)$$

Referring to equation (2), it should be remembered that β_p depends strongly on $\lambda_{T,p}$ and N and only weakly on Re_ϕ. For a given value of β_p, $\lambda_{T,p}$ doubles when N is increased from 12 to 24. Fig. 7 shows that, for a given value of β_p, $\beta_{\infty,b}$ decreases as N decreases. Larger numbers of nozzles and larger values of flow rate are expected to reduce the mixing losses, but it is not possible here to differentiate between the effects of N and $\lambda_{T,p}$.

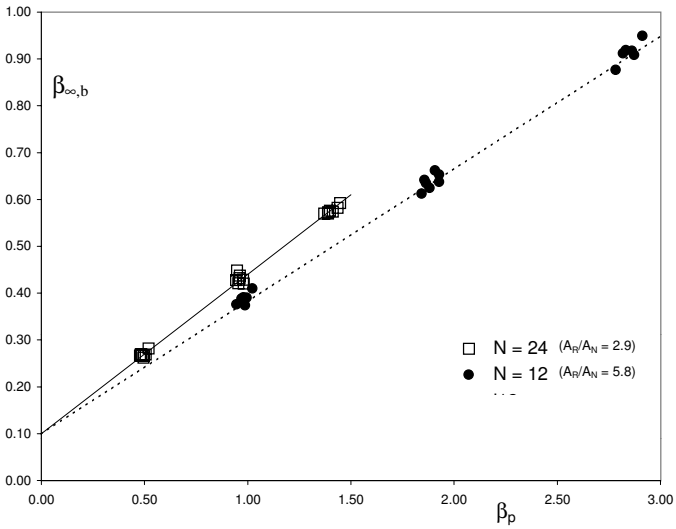

Fig. 7 Measured variation of $\beta_{\infty,b}$ with β_p

(------ equation 4a, ——— equation 4b)

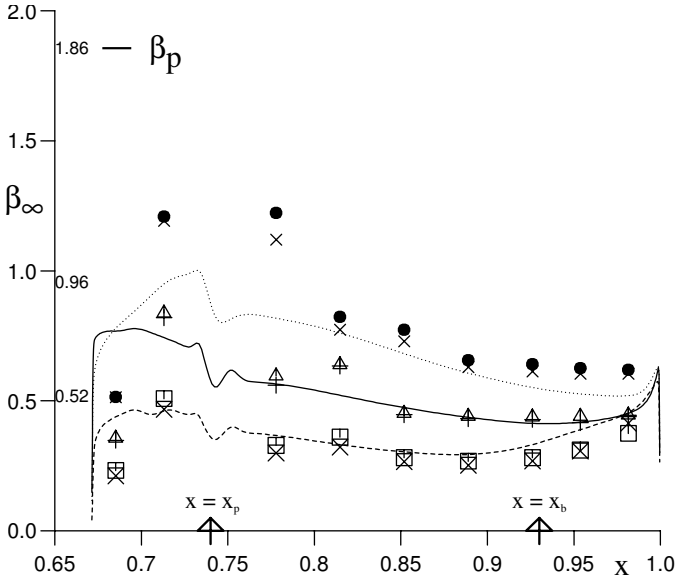

Fig. 6 Effect of β_p and $\lambda_{T,p}$ on measured and computed variation of β_∞ (z/s = 0.5)

measured ($Re_\phi \approx 0.78\text{x}10^6$, $1.2\text{x}10^6$)		computed (N = 24) ($Re_\phi = 0.78\text{x}10^6$)
□ , ⧖	$\lambda_{T,p} \approx 0.127$, $\beta_p \approx 0.52$, N = 24	------
△ , +	$\lambda_{T,p} \approx 0.236$, $\beta_p \approx 0.96$, N = 24	———
● , x	$\lambda_{T,p} \approx 0.229$, $\beta_p \approx 1.86$, N = 12	.....

Measured discharge coefficients

Definition of C_D for receiver holes. C_D is defined here as:

$$C_D = \frac{\dot{m}_b}{\dot{m}_i} \qquad (5)$$

where $\dot{m}_b$ is the measured mass flow rate through the receiver holes and $\dot{m}_i$ is the isentropic value.

Consider the isentropic flow in a stream tube from station 1 to station 2 in a rotating fluid. The work done *by* the air, $\dot{W}_{12}$, is given by

$$-\frac{\dot{W}_{12}}{\dot{m}_i} = \Omega(r_2 V_{\phi,2} - r_1 V_{\phi,1}) = c_p(T_{0,2} - T_{0,1}) \qquad (6)$$

where T_0, the total temperature in a *stationary* frame of reference, is

$$c_p T_0 = c_p T + \tfrac{1}{2} U^2 \qquad (7)$$

T being the static temperature and U the magnitude of the velocity in a stationary frame.

It is convenient to locate station 1 in the rotating core of fluid and station 2 at the outlet of the receiver holes, such that $r_2 = r_b$. It can be shown from equation (6) that, for isentropic flow of a perfect gas,

$$\frac{\dot{m}_i}{A_2} = \rho_{0,1}\left(\frac{p_2}{p_{0,1}}\right)^{\frac{1}{\gamma}}\left\{\left(\frac{2\gamma}{\gamma-1}\right)\frac{p_{0,1}}{\rho_{0,1}}\left[1-\left(\frac{p_2}{p_{0,1}}\right)^{\frac{\gamma-1}{\gamma}}\right] + 2\Omega(r_2 V_{\phi,2} - r_1 V_{\phi,1}) - V_{\phi,2}^2\right\}^{1/2} \qquad (8)$$

For the case where $V_{\phi,1} = V_{\phi,2} = 0$, equation (8) reduces to the standard result for flow through a stationary nozzle. When $r_1 = r_2$, equation (8) is equivalent to the result used by those authors (see, for example Dittmann et al (6)) who base C_D on *relative* total pressure rather than the *absolute* value used here. It should be emphasised that the use of relative pressures is *only* valid if $r_1 = r_2$, which may not be true in all cases. It can also be shown that, for any value of $V_{\phi,1}$, $\dot{m}_i$ will have a maximum value when $V_{\phi,2} = \Omega r_2$.

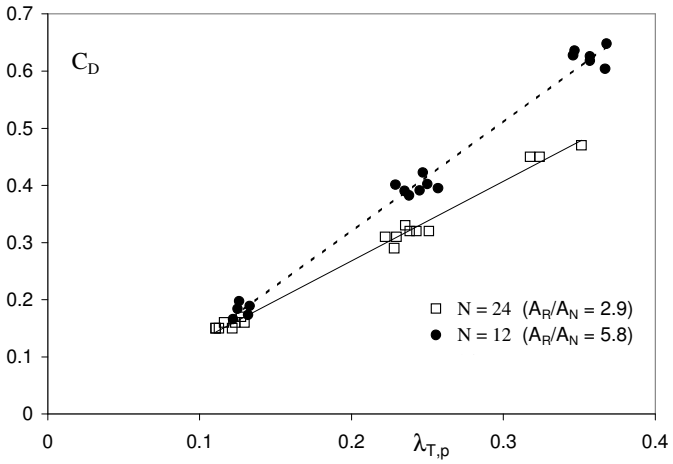

Fig. 8a Measured variation of C_D with $\lambda_{T,p}$

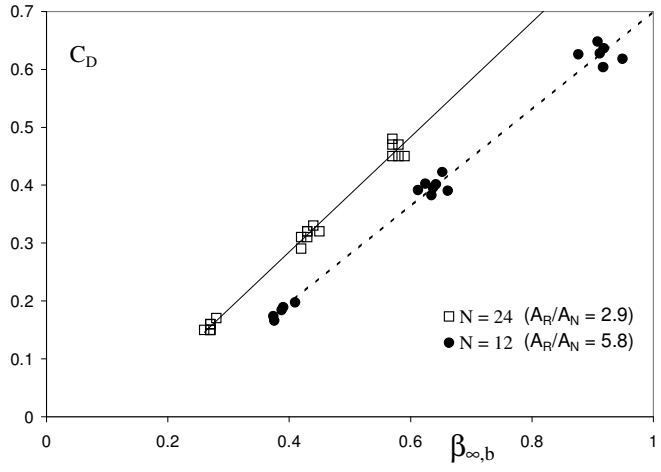

Fig. 8b Measured variation of C_D with $\beta_{\infty,b}$

Measurement of C_D. It should be noted that, owing to an error in processing the experimental data, the versions of Figs 8a and 8b presented in the conference paper GT-2002-30415 are incorrect. The corrected versions of these figures are presented here, and the text below has been modified accordingly.

In the results discussed here, $p_{0,1}$ and $V_{\phi,1}$ were respectively taken as the total pressure and tangential component of velocity measured by the pitot tube at $r = r_b$. Also, $V_{\phi,2}$ was assumed to be equal to Ωr_b (the rotational speed of the receiver holes), and p_2 was taken as the atmospheric pressure.

In measurements of C_D in rotating discs, experimenters usually assume, explicitly or implicitly, that the swirling air achieves solid-body rotation at exit from the receiver holes, as is assumed here. If the length-to-diameter ratio of the receiver holes is sufficiently large then this assumption will be valid; in the rig used here, the length-to-diameter ratio is 1.25 and so the assumption is questionable. As noted above, $\dot{m}_i$ calculated from equation (8) will be a maximum when $V_{\phi,2} = \Omega r_2$. That is, the assumption that $V_{\phi,2} = \Omega r_2$ will produce a lower bound for the true value of C_D; an upper bound could be found by setting $V_{\phi,2} = V_{\phi,1}$ in equation (8).

It is expected that C_D will be a maximum when the air near the receiver holes is in synchronous rotation with the disc, i.e. when $\beta_{\infty,b} = 1$; the air will then enter the holes with minimum shear. It is also expected that higher values of C_D will occur the more uniform is the distribution of flow between the receiver holes. As the number N of inlet pre-swirl nozzles is reduced (hence as the ratio A_R/A_N increases), the distribution of the discrete inlet flows to the receiver holes is likely to become less uniform, and values of C_D would be expected to decrease.

Figs 8a and 8b respectively show the variation of C_D with $\lambda_{T,p}$ and with $\beta_{\infty,b}$. Fig. 8a shows that C_D increases as $\lambda_{T,p}$ increases and, for any value of $\lambda_{T,p}$, C_D is larger for N = 12 than for N = 24. It should be remembered that, for a given value of $\lambda_{T,p}$, β_p increases as N decreases: the effects of N and β_p are therefore coupled in the experiments.

Fig. 8b shows that, as expected, C_D increases as $\beta_{\infty,b}$ increases; also, for a given value of $\beta_{\infty,b}$, C_D decreases as N decreases. Linear extrapolation (which may not be appropriate) to $\beta_{\infty,b} = 1$ suggests that $C_D \approx 0.7$ for N = 12 ($A_R/A_N = 5.8$), and $C_D \approx 0.9$ for N = 24 ($A_R/A_N = 2.9$). These values are consistent with the results of Popp et al (1), who also found that C_D decreases as A_R/A_N increases. Their maximum values of C_D, at $\beta_{\infty,b} = 1$, were 0.53 and 0.8 for $A_R/A_N = 7$ and 2 respectively.

Dittman et al (6) found that, for a given number of nozzles (N=11 or 12), C_D increased as the number of receiver holes increased (from 4 to 24), which is consistent with the "uniformity" argument. They also showed that, as expected, radiusing the inlet of the receiver holes increased C_D. It is difficult to make quantitative comparisons with their measurements, as they based their values of C_D on predicted rather than measured values of pressure in the core.

CONCLUSIONS

Measurements and three-dimensional steady computations have been carried out for the fluid dynamics of a compact pre-swirl rotor-stator chamber, simulating part of the blade-cooling air supply system used in some gas-turbine engines. The effects of rotational speed, flow rate, pre-swirl ratio and number of pre-swirl nozzles on the flow field and on the total pressure losses in the system were investigated.

Turbulent flow computations, carried out using a simplified 3D steady model of the system, gave results for total pressure and tangential velocity which were in mostly good agreement with measurements in the outer part of the system (including the radial location of the receiver holes). It was shown that, owing to mixing losses, there is a significant drop in total pressure between the pre-swirl nozzles and the core of rotating fluid. Consequently, the measured and computed values of swirl ratio, β_∞ (outside the boundary layers on the disc surfaces), were significantly lower than the inlet pre-swirl ratio, β_p. Measurements showed that, at the radius r_b of the receiver holes in the rotating disc, $\beta_{\infty,b}$ increased linearly with increasing β_p , and the ratio was higher for N = 24 pre-swirl nozzles than for N = 12; it should be noted that, for the same value of β_p, the flow rate for N = 24 is double that for N = 12. Discharge coefficients, C_D, were measured assuming solid-body rotation for the flow inside the receiver holes. As expected, C_D increased as $\beta_{\infty,b}$ increased. For a given value of $\beta_{\infty,b}$, C_D decreased as N decreased.

ACKNOWLEDGMENTS

The experimental work described here was funded by Alstom Power Ltd and the UK Engineering and Physical Sciences Research Council (EPSRC). Mr Farzaneh-Gord is a PhD student funded by the Iranian Government.

REFERENCES

1. Popp, O., Zimmerman, H. and Kutz, J, 1998, CFD analysis of cover-plate receiver flow, J. Turbomachinery, v. 120, pp 43-49
2. Karabay, H., Chen, J. X., Pilbrow, R., Wilson, M. and Owen, J. M., 1999, Flow in a "cover-plate" pre-swirl rotor-stator system, J. Turbomachinery, v. 121, pp 160-166
3. Karabay, H., Wilson, M. and Owen, J. M., 2001, Predictions of effect of swirl on flow and heat transfer in a rotating cavity, Int. J. Heat and Fluid Flow, v. 22, n. 2, pp 143-155
4. Meierhofer, B. and Franklin, C.J., 1981, An investigation of a preswirled cooling airflow to a gas turbine disk by measuring the air temperature in the rotating channels, ASME Paper 81-GT-132.
5. Wilson, M, Pilbrow, R. and Owen, J. M., 1997, Flow and heat transfer in a pre-swirl rotor-stator system, J. Turbomachinery, v. 119, pp 364-373
6. Dittmann, M., Geis, T., Schramm, V., Kim, S. and Wittig S., 2001, Discharge coefficients of a pre-swirl system in secondary air systems, ASME paper 2001-GT-122
7 Owen, J.M. and Rogers, R.H., 1989, Flow and heat transfer in rotating disc systems: Vol. 1, Rotor-stator systems, Research Studies Press, Taunton, UK and John Wiley, NY
8. Launder, B. E. and Sharma, B. I., 1974, Application of the energy-dissipation model of turbulence to flow near a spinning disc, Letters in Heat and Mass Transfer, 1974, 1, 131-138
9. Pilbrow, R., Karabay, H., Wilson, M. and Owen, J. M., 1999, Heat transfer in a "cover-plate" pre-swirl rotating-disc system, J. Turbomachinery, v. 121, pp 249-256